RSC Advances

ROYAL SOCIETY OF CHEMISTRY

www.rsc.org/advances

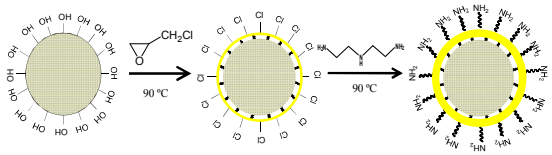

A potentially low-cost modified sawdust (MSD) effective for rapid Cr(VI) and As(V) removal from water.

A potentially low-cost modified sawdust (MSD) effective for rapid Cr(VI) and As(V) removal from water

Linlin Hao[a], Qin Liu[a], Xilan Li[b], Zhaolin Du[a] ,Peng Wang[a] *

[a] State Key Laboratory of Urban Water Resource and Environment, School of Municipal and Environmental Engineering, Harbin Institute of Technology, Harbin 150090, P. R. China

[b] State Key Laboratory of Physical Chemistry of Solid Surfaces, College of Chemistry and Chemical Engineering, Xiamen University, Xiamen 361005, P. R. China

* Corresponding author. Tel.: 86-13945181528; fax: 86-451-86283801

E-mail address: pwang73@vip.sina.com (Peng Wang)

Abstract

The study was investigated to evaluate the effectiveness of diethylenetriamine (DETA)-crosslinked adsorbent prepared from pine sawdust in removing Cr(VI) and As(V) from aqueous solutions. The maximum adsorption capacity of Cr(VI) and As(V) by MSD was highly enhanced from 7.04 mg/L to 238.6mg/g and from 4.88 to 71.23 mg/g respectively at pH 6.0. The surface characterization of the MSD proved that the grafted amino groups are responsible for the good affinity towards Cr(VI) and As(V). The uptake of Cr(VI) and As(V) was highly pH dependent and was facilitated in acidic solutions. Batch experiments were conducted as a funciton of pH, temperature and contact time. Both Cr(VI) and As(V) adsorption equilibrium could be quickly attained within 1 h and the process followed the Redlich-Peterson isotherm model. As(V) uptake was far more sensitive to the individual co-existing anion (Cl^-, SO_4^{2-}, NO_3^-, HCO_3^-) than Cr(VI). The mechanism was found to be electrostatic attraction between positively charged surface of sawdust and Cr(VI)/As(V) anions.

Keywords: Cr(VI) (chromate); As(V) (arsenate); Modified sawdust (MSD); Adsorption; Amino groups

1. Introduction

Chromate (Cr(VI)) or arsenate (As(V)) enrichment in aquatic environment is of great concern to people worldwide because of the chronic effects of poisoning on people who are exposed to high concentrations. Cr(VI) is highly toxic and the long time exposure at elevated concentrations can cause damage to liver, kidney and nerve tissue.[1, 2] The typical sympotoms of long-term exposure to arsenic associated with rise in various types of diseases (neurological, hematological, renal and skin diseases) and even cancers. In view of the adverse effect of environmental Cr(VI) and As(V), the World Health Organization (WHO) drinking water guidelines for total chromium and total arsenic are 0.05 mg/L and 0.01 mg/L respectively.

The concentrations of arsenic above 0.01 mg/L may be naturally caused by certain special geological conditions, the occurrences of arsenic at elevated concentration in groundwater were reported by many literatures.[3-5] For example, the groundwater from Datong Basin (China) was detected with arsenic concentration up to 1.55 mg/L.[6] However, the high levels of Cr(VI) or As(V) discharged into water bodies are more commonly caused by industrial activities, such as leather tanning, mining, electroplating, and metal smelting industries.[7]

Among many technologies available for Cr(VI) or As(V) removal from water, chemical precipitation is a conventional remediation technology, which typically involve reduction of Cr(VI) to Cr(III) and subsequent precipitate as sludge at high pHs. However, it is commonly applied to the wastewater with very high Cr(VI) or As(V) concentrations and could not remove them satisfactorily to meet the

discharge standards. For instance, the As(V) removal from water via chemical precipitation induced by adding lime can only reduce solution As(V) concentration to a level of 1–5 mg/L, still much higher than the drinking water standard (0.01 mg/L). Moreover, the production of large amount of toxic sludge cannot be negligible.

In recent years, considerable studies have focused on the removal of Cr(VI) or As(V) via adsorption. Various types of adsorbents have been reported including activated carbons, metal oxide, polymeric adsorbents and biocomposites (mycelium, bacteria, agriculture waste, etc.).[8-10] In particular, biomass adsorbents have gained considerable attention due to the very low cost and great potential to be modified as type of highly efficient adsorbent. In this study, sawdust (approximately US$ 0.02-US$ 0.09, china) is selected as a host material because it is produced in large quantities as a solid waste at sawmills. In addition, sawdust contains mainly lignocellulose and it was reported that the cellulose content of oak (*Quercus coccifera*) sawdust was 41.5%.[11] A variety of functional groups such as hydroxyl group make it possible to react with other moieties for enhancement in the efficiencies of metal ions adsorption. Novel adsorbents of modified Sawdust have been reported by many studies. Ansari and Fahim modified the sawdust by coating with polypyrrole in order to get an anion exchanger material.[12] The synthetic route was simple and the modified sawdust was showed to be an effective adsorbent to remove Cr(VI) from aqueous solutions. Bajpai, etc. also prepared the modified sawdust by coating with polypyrrole to remove phosphate from water.[13] Khalkhali, etc. investigated the removal of Cr(VI) from water using polyaniline coated sawdust.[14]

Previous studies have demonstrated the amino group was effective in the removal of metal anions.[15-17] In this study, a novel low-cost adsorbent material of MSD was developed for the adsorption of Cr(VI) and As(V) from water. The synthetic route includes two steps: etherification and crosslink reaction. A recent study reported that a crosslinked cornstalk was further grafted with triethylamine to obtain a kind of anion exchanger.[16] However, our study demonstrated that sawdust pariticles after crosslinked with DETA aggregated all together and it was impossible to further react with triethylamine. We got the adsorption performance for Cr(VI) almost as good as the triethylamine grafted cornstalk, meanwhile the synthetic procedure is simplified. The SEM results showed obviously that a thin organic film was covered on the surface of sawdust but it does not mean that any other kinds of supporters are appropriate because the former etherification reaction between lignocellulose hydroxyl and epichlorohydrin (ECH) is a key step which makes possible for the following cross-linking reaction.

2. Materials and methods

2.1 Reagents and stock solutions

A stock solutions of 1000 mg/L Cr(VI) and 1000 mg/L As(V) were prepared by $K_2Cr_2O_7$ (AR quality), Na_2HAsO_4 (AR quality) and deionized water. 0.1，0.01M NaOH solutions and 0.1, 0.01M HNO_3 solutions was prepared by sodium hydroxide (AR quality) and nitric acid (AR quality) to adjust the pH values. Cr(VI) samples of various concentrations were all prepared with deionized water. The organic reagents (ECH, DMF, DETA, etc.) used in the synthesis process were all analytical reagents.

2.2 Preparation of crosslinked sawdust

The sawdust was seized through 40 mesh screen and washed with deionized water to remove impurities. 3 g of pretreated sawdust was dispersed in mixture solutions of 20 mL N, N-Dimethylformamide (DMF) and 15 mL ECH in a three necked flask, kept in a constant-temperature water-bath at 90°C for 1 h. The crosslinking agent of 5 mL diethylenetriamine (DETA) was dropwise added into the flask and kept for 1 h. Finally the mixture was filtered and the precipitated product was washed with absolute ethyl alcohol, then dried. The synthesis route is shown in Fig. 1.

2.3 Batch experiments

2.3.1 Isotherm study

Batch experiments were carried out by reacting 100 mL various concentrations of $K_2Cr_2O_7$ or Na_2HAsO_4 solution with 0.2 g MSD at pH 6.0 and room temperature. The isotherm experiments were conducted with initial Cr(VI) and As(V) concentrations 1 to 200 mg/L.

2.3.2 Kinetics

The effect of contact time on Cr(VI) and As(V) removal was investigated with 10, 50, and 100 mg/L of Cr(VI) and As(V) solutions. The experiments were conducted in a round glass reactor that was placed in a thermostatic water bath where the temperature could be adjusted to different degrees. A pH electrode combined with a thermometer was inserted into the reactor solution to detect the pH and temperature change. The samples were collected at certain time intervals.

2.3.3 Effect of pH and co-existing anions

The solution pH (100 mg/L Cr(VI) and 50 mg/L As(V)) was adjusted with the addition of NaOH or HNO_3 solution to obtain pH range of 2-11. The samples were adjusted several times at the starting 2 h to maintain the desired pH to be stable. The co-existing anions were prepared including Cl^-, SO_4^{2-}, NO_3^- and HCO_3^-.

2.3.4 Fixed-bed column run

The packed column experiments were conducted using a glass column of 22×200 mm, column was packed with certain dosage of MSD to obtain the different bed depths. A nylon mesh (200 μm opening size) was palced at the bottom of the glass column to prevent sawdust from being discharged into the tubing. 10 mg/L Cr(VI) or 2.5 mg/L As(V) solution at natural pH was pumped through the column at a desired flow rate (10.1 mL/min) with a peristaltic pump. Effluent samples were collected at regular time intervals to determine Cr(VI) or As(V) concentration in the effluent solutions.

2.4 Analysis methods

The FTIR spectra was obtained with UV2550 (Shimadzu Co., Ltd., Japan) using a KBr disc as background over the range of 450–4000 cm^{-1}. The mass ratio between the sample and KBr powder is about 1: 100. The SEM images were obtained using Quanta 200 FEG (USA), which was coupled with EDS system. The BET surface areas were determined by an instrument of ASAP 2020 Accelerated Surface Area and Porosometry System (Global Spec. Inc., US). All samples were analyzed using inductively coupled plasma - optical emission spectroscopy (ICP-OES) (PerkinElmer, Optima 2000, UK).

3. Results and discussion

3.1 Surface properties of MSD

3.1.1 FTIR analysis

The FTIR was carried out to investigate the surface properties of raw sawdust and MSD. As shown in Fig. 2, the broad band of 3310 cm^{-1} represented the –OH groups. The peak at 2918 cm^{-1} in raw sawdust is associated with the special vibration of C–H aliphatic. The peak at 1738, 1640 and 1503 cm^{-1} in raw sawdust could be assigned to the carboxylic groups. Pine sawdust consists mainly of lignocellulose, hemicelluloses, pectin, lipids and waxes, etc.[18] Carboxylic groups primarily presents in pectin subtance, lipids and waxes, the absence of the bands (1738, 1640 and 1503 cm^{-1}) which represent carboxylic groups may indicate these subtances have already been removed during the synthetic process. The peaks at 1555 cm^{-1} and 1542 cm^{-1} indicates the presence of amino groups on MSD. The intense vibration observed at 1370 and 1057 cm^{-1} in MSD could be assigned to C–N stretching vibration of amino groups. The functional groups before and after modification and the corresponding infrared adsorption bands are shown in Table 1.

3.1.2 Scanning Electron Microscopy

SEM analysis for the raw sawdust and MSD were performed to see clearly the surfaces of particles. The SEM photograph of the raw sawdust revealed the surface was abundant with regular pores of uniform size. After modification, the surface of sawdust was covered with a thin organic film as shown in Fig. 3. This result validates the increase trend of BET surface area from 0.122 to 0.156 m^2/g after modification. The similar trend was also observed by Keränen, etc.[18] who modified the pine

sawdust by means of ECH, ethylenediamine and triethylamine, the BET surface area (P_0/P=0.2) was increased from 0.836 to 1.44 m^2/g. The summary reports of surface areas of the raw sawdust and MSD were shown in Fig. S1. According to the SEM images, the organic film on MSD surface presented to be heterogeneous, so Site 1 (S1), Site 2 (S2) and Site 3 (S3) were selected for EDS analysis as shown in Fig. 3, a slight increase was observed in the C contents (54.62%—(56.14~57.78%)). However, N content increased significantly from 0.47% to 8.91~13.80%, indicating that a large number of amine groups have been introduced onto the sawdust surface, N content of MSD varied from 8.91% of S1 to 13.80% of S3, this larger fluctuation could be contributed to the side reaction during the synthetic process or the incomplete reaction. The Cl content of MSD slightly fluctuated in a range of 14.63%-17.33%, which was due to the excess dosage of ECH reagent. The elemental composition of EDS analysis was shown in Table. 2.

3.2 Batch studies

3.2.1 Effects of solution pH on Cr(VI) and As(V) adsorption

It is important to study the effect of pH on the removal of Cr(VI)/As(V) onto MSD. Cr(VI) or As(V) anion is not a simple monovalent anion but rather a series of anions depending on the pH. Also the solution pH affects the surface charge of the adsorbent. Cr(VI) or As(V) speciation is affected by the solution pH through the following equilibrium:

$$HCrO_4^- \longleftrightarrow CrO_4^{2-} + H^+ \qquad pK_a = 5.9 \qquad (1)$$

$$H_2CrO_4^- \longleftrightarrow HCrO_4^{2-} + H^+ \qquad pK_a = 4.1 \qquad (2)$$

$$Cr_2O_7^{2-} + H_2O \longleftrightarrow 2HCrO_4^- \quad pK_a = 2.2 \quad (3)$$

$$H_3AsO_4 \longleftrightarrow H_2AsO_4^- + H^+ \quad pK_a = 2.3 \quad (4)$$

$$H_2AsO_4^- \longleftrightarrow HAsO_4^{2-} + H^+ \quad pK_a = 6.8 \quad (5)$$

$$HAsO_4^{2-} \longleftrightarrow AsO_4^{3-} + H^+ \quad pK_a = 11.6 \quad (6)$$

The pH influence on the adsorption was shown in Fig. 4, Cr(VI) removal efficiency was kept constant in neutral and acidic conditions (pH range of 2.0–6.0) but significantly decreased from pH 7.0 to 12. The maximum Cr(VI) adsorption capacity (97.91 mg/g) was found at lower pHs between 2 and 6. A different trend was observed for As(V) adsorption, the optimal pH was found between 4 and 6. When pH was lowered from 4 to 2, a gradual decrease is observed from 91.8% to 79.2%. According to Eq.(4), As(V) species at pH 2 ~ 3 exists mostly as neutral form (H_3AsO_4). From Eqs. (5) to (6), the As(V) species occurs mainly in the form of $H_2AsO_4^-$ in the pH range between 3 and 6, while a divalent anion $HAsO_4^{2-}$ dominates at higher pH values (pH 7 ~ 11). The high concentration of H^+ causes the protonation of MSD surface and then strengthen the electrostatic attraction forces between amino groups and As(V) species. As pH increases from 3 to 6, the increase of concentrations of $H_2AsO_4^-$ and $H_2AsO_4^-$ will enhance electrostatic attraction between anion exchanger and arsenate. When the pH increases from 7 to 10.0, the increase of concentration of OH^- will significantly decrease the protonation effect of amino groups, also the excess OH^- ions will compete with arsenate for sorption sites.

3.2.2 Adsorption kinetics

In order to define the adsorption rate and the contact time required to get equilibrium,

the kinetic parameters were studied by monitoring the adsorption capacities of Cr(VI) and As(V) in certain time interval. The Cr(VI) adsorption kinetic experiments under the temperature of 10, 30, 50°C with initial concentration of 50 mg/L were illustrated in Fig. 5. The slope of the three curves gradually became steep, indicating the reaction rate increased with a rise in temperature. The Cr(VI) concentration in solution reached its lowest level (0.65 mg/L) quickly within around 30 min. The reaction rate of As(V) is also very quick and the equilibrium is reached within around 40 min. It can be observed that the rate of Cr(VI) adsorption on MSD was faster than As(V), the adsorption rate constants at 30°C for Cr(VI) and As(V) with the same initial concentration of 50 mg/L are 9.7 mg/g • min and 3.8 mg/g • min respectively. The adsorption rate constant v_0 can be obtained from the following:

$$v_0 = k_2 q_e^2 \tag{7}$$

For other batch experiments, the contact time was maintained as 1 h.

The data were regressed against pseudo-first-order, pseudo-second-order and intraparticle diffusion equations (Eq. (8)-(10)).

$$\log(q_e - q_t) = (\log q_e) - k_1 t \tag{8}$$

$$\frac{t}{q_t} = \frac{1}{k_2 q_e^2} + \frac{1}{q_e} t \tag{9}$$

$$q_t = k_d t^{1/2} + C \tag{10}$$

Where q_t is the quantity of Cr(VI) or As(V) adsorbed at time t (mg/g), q_e the quantity of Cr(VI) or As(V) adsorbed at equilibrium (mg/g), k_1 (min^{-1}), k_2 (g • mg^{-1} •min^{-1}) and k_d (mg • L^{-1} • $min^{-1/2}$) are the rate constants of the first-order, pseudo-second-order and intraparticle diffusion equations, respectively.

There are three main stages in the process of adsorption by adsorbents: (1) mass transfer across the external boundary layer; (2) diffusion within the pores of the adsorbent; (3) adsorption at a special site on the surface.[19] The external mass-transfer constant (k_s) involving stage (1) is calculated from the initial slope of the curve C_t/C_0 versus t according to the following equation:

$$[\frac{d(C_t/C_0)}{dt}] = k_s S \quad (11)$$

The higher values of k_s indicated a decrease in the resistance of the boundary film to mass transfer. The agitation condition of the liquid-solid system caused a decrease in the thickness of the diffusion layer at the adsorbent surface with a consequent increase in the mass-transfer coefficient.[20] The intraparticle diffusion rate constant (k_d) was calculated from Eq. (10). For any porous material, the intraparticle diffusion involves stage (2) usually plays a more important role than surface diffusion, a larger k_d and better conformation to intraparticle equation represents that intraparticle diffusion is the rate-limiting process for adsorption.

As shown in Table 2, the entire kinetic data were best fitted to the pseudo-second-order model, indicating that the adsorption process followed the second-order chemisorptions.[21] The correlation coefficients R^2 of less than 0.73 indicated the bad fit to the intraparticle diffusion equation, because MSD has a very small percentage of micropores, mesopores and transitional pores, the surface areas of 0.156 m^2/g was mainly attributed to the external surface area.

3.2.3 Adsorption isotherms

Adsorption isotherms at three different temperatures (10, 30, and 50°C) were obtained

to study the thermodynamic process. As shown in Fig. 6, the maximum Cr(VI) adsorption capacity of MSD at 50°C reached 238.6 mg/g while As(V) achieved that maximum adsorption capacity of 71.23 mg/g. Temperature played an important role in determining the maximum adsorption capacity. As shown in Table 3, the isotherm data fitted the Langmuir model well ($R^2 > 0.97$). Both the K_L and q_e values increased as the temperature increased, indicating the endothermic nature of Cr(VI)/As(V) adsorption on MSD.

The adsorption equilibrium data were fitted with Langmuir, Freundlich and Redlich–Peterson models. The Langmuir isotherm is derived from the assumption that monolayer adsorption takes place on a homogeneous adsorbent surface with identical adsorption sites. The Langmuir isotherm equation is expressed below: [21]

$$\frac{C_e}{q_e} = \frac{C_e}{q_{\max}} + \frac{1}{q_{\max} K_L} \quad (12)$$

Where q_e is the quantity of the species adsorbed at equilibrium (mg/g), K_L is a constant representing the virtual bonding strength between the target species and adsorbent, C_e is the equilibrium concentration of adsorbate in the solution, $q_{\max}$ is the maximum adsorption capacity.

The assumption of Freundlich isotherm is that the adsorbent surface is distributed with heterogeneous adsorptive energies. The Freundlich isotherm equation was expressed as follows:

$$\ln q_e = \ln K_F + 1/n \ln C_e \quad (13)$$

Where q_e is the quantity of the species adsorbed at equilibrium (mg/g), K_F is a constant which is a measure of adsorption capacity, $1/n$ is a measure of adsorption

density, C_e is the equilibrium concentration of adsorbate in the solution.

Redlich–Peterson model incorporates the advantages of both Langmuir and Freundlich models, which approaches Freundlich model at high concentrations and accords well with Langmuir model at low concentrations.[22] Redlich–Peterson equation can be written as:

$$q_e = \frac{K_{RP} C_e}{1 + \alpha C_e^{\beta}} \quad (14)$$

Where K_{RP} is Redlich–Peterson equation constant, β is the exponent which lies between 0 and 1. The linear form of R-P isotherm equation is:

$$\ln\left(\frac{K_{RP} C_e}{q_e} - 1\right) = \ln \alpha + \beta \ln C_e \quad (15)$$

The adsorption of Cr(VI) or As(V) fitted very well with the Langmuir isotherm model with the coefficient of determination (R^2) for each set of the linearized data above 0.96 as shown in Table. 4.

Fig. S2 showed the raw sawdust had little affinity for Cr(VI) and As(V). In contrast, the MSD showed an excellent performance for Cr(VI) or As(V) adsorption. The noteworthy difference indicated that amino groups have good affinity for Cr(VI) and As(V). Since the MSD has the much lower BET specific surface area (0.156 m^2/g) than the strong base anion exchange resin (D211) (66.7 m^2/g), the high adsorption capacity was exactly attributed to the high density of crosslinking amino groups.

3.2.4 Effects of co-existing anions on Cr(VI) and As(V) adsorption

In natural water sources such as rivers and lakes, many anions might exist together. In our study, the adsorption of Cr(VI) and As(V) on MSD have been studied in presence

of various inorganic anions including SO_4^{2-}, NO_3^-, Cl^- and HCO_3^-. Fig. 7 showed the effects of these competing ions on the removal of Cr(VI) and As(V). The presence of NO_3^- or Cl^-, even at high concentrations, had almost no negative effect on the adsorption capacity of Cr(VI). SO_4^{2-} at 100 mg/L slightly affected the removal of Cr(VI). HCO_3^- had a stronger effect than other three anions. For As(V), the presence of SO_4^{2-}, NO_3^-, Cl^-, HCO_3^- respectively had resulted in a great reduction in As(V) removal efficiency. It was observed that individual SO_4^{2-} (10 mg/L), NO_3^-(10 mg/L), Cl^- (10 mg/L), HCO_3^- has resulted in 18%, 22%, 24%, 28% respectively reduction in As(V) uptake, the occurrence of SO_4^{2-} up to 100 mg/g has shown 74% reduction in As(V) uptake. All these anions affected the Cr(VI) or As(V) adsorption process via their competition for electrostatic attraction. According to the results, the following order of magnitude of the interfering effects on MSD was obtained:

$$Cr_2O_7^{2-} > HCO_3^- > SO_4^{2-} > NO_3^- > Cl^- > H_2AsO_4^- \quad (16)$$

which was a little different with the order of selectivity on the strong base anion exchange resin:

$$Cr_2O_7^{2-} > SO_4^{2-} > NO_3^- > Cl^- > HCO_3^- \quad (17)$$

3.3 Fixed bed column runs

Fig. 8 showed the breakthrough curves at different bed depths. The flow rate was kept constant at 10.1 mL/min, It was clear that the bed depth strongly influenced the Cr(VI) adsorption capacity, both the exhaustion time and effluent volume (V_{eff}) increased as the bed depth increased. The slope of breakthrough curve decreased with an increase in bed depth, which was attributed to the broadened mass transfer zone.[23] The

adsorption column data were evaluated and presented in Table 5. The Cr(VI) adsorption capacity of 167, 164 and 154 mg/g were recorded at 1.8, 2.3 and 2.8 cm, respectively. It was shown that the shorter bed depth of 1.8 cm offered an optimum breakthrough curve and the highest adsorption capacity of 167 mg/g for Cr(VI). As(V) showed a similar trend of the breakthrough behavour, the adsorption capacity of As(V) decreased from 75 mg/g to 69 mg/g with an increase of the bed depth from 1.5 to 2.6 cm.

Several models were widely used to simulate the column tests data, i.e. thomas, Yoon-Nelson, Wolborska and Adams–Bohart models. In this study, bed depth service time (BDST) approach based on Adams–Bohart equation, which was proved to be the most successful method of analyzing data of column runs,[24, 25] was used to fit the column experiment data, the model was described as the following equation:

$$t = \frac{N_0}{C_0 V} X - \frac{1}{C_0 K} \ln\left(\frac{C_0}{C_t} - 1\right) \quad (18)$$

Where C_0 is the initial concentration of solute (mg/L), N_0 means the saturation concentration of the column bed (mg/L), C_t the desired concentration of solute at breakthrough (mg/L), K_a the adsorption rate constant (L/mg • h), X the column bed depth (cm), V represents the empty bed flow linear velocity (cm/h), t the service time of column under obove conditions (h). Service time t corresponds to the effluent concentration of 0.05 mg/L for Cr(VI) and 0.01 mg/L for As(V) according to the drinking water standards.

The BDST model is in the form of

$$t = aX + b \quad (19)$$

Where

$$a = \frac{N_0}{C_0 V} \tag{20}$$

$$b = -\frac{1}{KC_0} \ln\left(\frac{C_0}{C_t} - 1\right) \tag{21}$$

The parameter N_0 and K_a can be calculated from the slope of the linear plot of t versus X as shown in Table 5.

If setting $t = 0$ and solving Eq. (19) for X yields:

$$X_0 = \frac{V}{KN_0} \ln\left(\frac{C_0}{C_t} - 1\right) \tag{22}$$

Where X_0 is the minimum bed depth allowing an effluent concentration C_t, known as the critical bed depth. The variation of the service time with bed depth is linearized in Fig. S3.

The details of fitted equations between the service time (t) and the bed depth (X) are given in Table 5. The critical depth value obtained for Cr(VI) and As(V) from the BDST model was 0.35 cm and 0.12 cm, respectively.

3.4 Mechanism for chromate and arsenate removal

According to the aforementioned results, we proposed that Cr(VI) and As(V) removal mechanisms might be electrostatic attraction as shown in Eqs. (23) and (24). At acid pH values, the surface charge of MSD was positive due to the protonation effect of amine groups, then the electrostatic attraction between protonated amine groups and Cr(VI)/As(V) anions contributed to the removal reaction.

$$—NH_3^+ \bullet\bullet\bullet R^- + HCrO_4^- \longleftrightarrow —NH_3^+ \bullet\bullet\bullet HCrO_4^- + R^- \tag{23}$$

$$—NH_3^+ \bullet\bullet\bullet R^- + H_2AsO_4^- \longleftrightarrow —NH_3^+ \bullet\bullet\bullet H_2AsO_4^- + R^- \tag{24}$$

This mechanism also explains the adsorption process is highly pH dependent and the removal performance decreased significantly in alkaline conditions.

Conclusion

The adsorption capacity of MSD for Cr(VI) and As(V) increased significantly when the raw material was crosslinked with DETA. Solution pH played a key role in the removal of Cr(VI) and As(V) from water, the maximum adsorption can be achieved at pH 2-6 for Cr(VI) and pH 5-6 for As(V). Temperature also plays an important role and the Cr(VI) adsorption capacities increased with a rise in temperature from 10 to 50°C. The kinetic data can be well described by the pseudo-second-order model, indicating the sorption process follows a second-order chemisorption. The adsorption isotherm can be well defined by Redlich-Peterson model. The MSD exhibits the co-existing anion selectivity sequence as bicarbonate > sulfate > nitrate > chloride. The mechanism of the removal of Cr(VI) and As(V) involves mainly through electrostatic attraction between anions and positively charged amine sites.

Acknowledgments

This work was supported by the Funds for Creative Research Groups of China (Grant No. 51121062) National Water Pollution Control and Management Technology Major Projects (2012ZX07205-005). Thanks very much for Emily's language reversion.

Reference

1 M. Owlad, M. K. Aroua, W. A. W. Daud, S. Baroutian, *Water, air, and soil pollution*, 2009, **200**, 59-77.

2 J. Kotaś, Z. Stasicka, *Environ. Pollut.*, 2000, **107**, 263-283.

3 N. E. Korte, Q. Fernando, *Crit. Rev. Env. Sci. Tec*, 1991, **21**, 1-39.

4 D. K. Nordstrom, *Science(Washington)*, 2002, **296**, 2143-2145.

5 P. Smedley, D. Kinniburgh, *Appl. Geochem.*, 2002, **17**, 517-568.

6 Y. Deng, Y. Wang, T. Ma, *Appl. Geochem.*, 2009, **24**, 587-599.

7 O. V. Lushchak, O. I. Kubrak, O. V. Lozinsky, J. M. Storey, K. B. Storey, V. I. Lushchak, *Aquat. Toxicol.*, 2009, **93**, 45-52.

8 X. Dou, R. Li, B. Zhao, W. Liang, *J. Hazard. Mater.*, 2010, **182**, 108-114.

9 S. R. Chowdhury, E. K. Yanful, *J. Environ. Manage.*, 2010, **91**, 2238-2247.

10 F. Fu, Q. Wang, *J. Environ. Manage.*, 2011, **92**, 407-418.

11 M. E. Argun, S. Dursun, C. Ozdemir, M. Karatas, *J. Hazard. Mater.*, 2007, **141**, 77-85.

12 R. Ansari, N. K. Fahim, *Reactive and Functional Polymers*, 2007, **67**, 367-374.

13 S. K. Bajpai, V. K. Rohit, M. Namdeo, *J. Appl. Polym. Sci.*, 2009, **111**, 3081-3088.

14 R. A. Khalkhali, A. R. Aliakbar, M. Masoudi, *J. Polym. Mater.*, 2005, **22**, 75-80.

15 X. Xu, B. Gao, W. Wang, Q. Yue, Y. Wang, S. Ni, *Colloids and Surfaces B: Biointerfaces*, 2009, **70**, 46-52.

16 S. Chen, Q. Yue, B. Gao, Q. Li, X. Xu, *Desalination*, 2011, **274**, 113-119.

17 A. M. Yusof, N. A. N. N. Malek, *J. Hazard. Mater.*, 2009, **162**, 1019-1024.

18 A. Keranen, T. Leiviska, B.-Y. Gao, O. Hormi, J. Tanskanen, *Chem. Eng. Sci.*, 2013, **98**, 59-68.

19 E. Malkoc, Y. Nuhoglu, M. Dundar, *J. Hazard. Mater.*, 2006, **138**, 142-151.

20 X. Xu, B.-Y. Gao, Q.-Y. Yue, Q.-Q. Zhong, X. Zhan, *Carbohydr. Polym.*, 2010, **82**, 1212-1218.

21 V. Vinodhini, N. Das, *American-Eurasian Journal of Scientific Research*, 2009, **4**, 324-329.

22 Z. Akmar Zakaria, M. Suratman, N. Mohammed, W. Azlina Ahmad, *Desalination*, 2009, **244**, 109-121.

23 M. A. Wahab, S. Jellali, N. Jedidi, *Bioresource Technol.*, 2010, **101**, 5070-5075.

24 Q.-S. Liu, T. Zheng, P. Wang, J.-P. Jiang, N. Li, *Chem. Eng. J.*, 2010, **157**, 348-356.

25 O. A. Fadali, *Adsorpt. Sci. Technol.*, 2003, **21**, 935-950.

Table 1

The FTIR spectral characteristics of sawdust before and after modification.

Wavelength range (cm^{-1})	RS	MSD	Assignment	Reference
3500-3300	3349	3312	Stretching –OH, -NH group	19
3000-2880	2918	2940	Aliphatic C-H group	20
1750-1680	1738	Absent	Stretching C=O	21
1670-1640	1640	1653	Carboxylic groups	22
1640-1500	1503	Absent		
1540-1640		1555	N-H bending (in plane)	This study
		1542		
1470-1400	1463	1456	O-H bending	21
1450-1375	1426	Absent	Symmetric bending of CH_3	19
1375-1300	1321	Absent	Stretching C-O	23
1400-1000	1244	Absent	O-H alcohols and aliphatic ether	23
1300-1000	1162	Absent	Stretching C-O of COOH	23
1370-1020		1370	Stretching C-N	23
		1057		
990-560	897	868	C-H bending	This study
	599	593		

Table 2

Elemental analysis of raw sawdust and MSD (% based on dry weight)

Element	Content (Wt%)			
	Raw sawdust	MSD		
		S1	S2	S3
C	54.62	57.78	56.14	56.28
O	42.71	18.69	14.39	12.59
N	0.47	08.91	12.46	13.80
Cl	0.2	14.63	17.01	17.33

Table 3

Kinetics models fitting parameters for Cr(VI)/As(V) adsorption on MSD at different temperature.

Species	*T/K*	Pseudo first-order		Pseudo second-order		Intraparticle diffusion			The external mass-transfer equation	
		k_1	R^2	k_2	v_0	R^2	k_d	R^2	k_s	R^2
Cr(VI)	283	0.062	0.993	0.012	7.87	0.999	1.41	0.610	0.073	0.929
	303	0.070	0.982	0.015	9.71	0.999	1.34	0.584	0.074	0.922
	323	0.073	0.989	0.016	10.64	0.999	1.32	0.573	0.075	0.945
As(V)	283	0.018	0.970	0.0058	3.82	0.999	1.589	0.731	0.047	0.939
	303	0.031	0.970	0.0071	4.69	0.999	1.548	0.690	0.050	0.937
	323	0.06	0.993	0.0089	5.88	0.999	1.489	0.654	0.052	0.923

Table 4

Freundlich, Langmuir and Redlich-Peterson isotherms constants of Cr(VI)/As(V) adsorption on MSD at different temperature.

Species	Langmuir isotherm				Freundlich isotherm			Redlich-Peterson			
	T/K	Q_{max}(mg/g)	k_L(L/mg)	R^2	n	K_F(mg/g)	R^2	K_{RP}	α	β	R^2
Cr(VI)	283	192.3	0.173	0.992	5.682	78.26	0.935	71	0.29	1.093	0.989
	303	232.6	0.187	0.985	5.464	86.49	0.958	225	1.94	0.906	0.999
	323	250	0.2	0.985	5.405	93.69	0.970	350	2.56	0.954	0.996
As(V)	283	68.97	0.279	0.994	1.661	8.662	0.875	33	0.78	0.886	0.993
	303	71.43	0.269	0.997	1.842	11.79	0.842	89	2.09	0.878	0.996
	323	76.92	0.25	0.997	1.876	13.80	0.827	105	2.02	0.915	0.999

Table 5

BDST parameters for sorption of Cr(VI) and As(V) at different bed depths.

Metal	Bed depth (cm)	Service time (h)	Fitted equation	R^2	N_0 (g/L)	K_a ($mg^{-1} \cdot h^{-1}$)	X_0 (cm)
Cr(VI)	1.8	50.1	$t = 40.54X+14.09$	0.998	19.56	0.037	0.35
	2.3	63.3					
	2.8	72.5					
As(Ⅴ)	1.5	75.4	$t = 22.4X+10.44$	0.989	10.8	0.21	0.12
	2.1	98.2					
	2.6	120.1					

Figure captions

Fig. 1 Schematic diagram of the synthesis process of MSD.

Fig. 2 FT-IR spectra of (a) Raw sawdust and (b) MSD.

Fig. 3 SEM images of raw sawdust and MSD.

Fig. 4 Effect of pH on Cr(VI) and As(V) removal by MSD. (Intial Cr(VI) and As(V) concentration were 100 mg/L and 50 mg/L respectively, MSD dosage 0.2g, temperature 25±2 °C.)

Fig. 5 Adsorption kinetics of Cr(VI) and As(V) by MSD at different temperatures. (Initial Cr(VI) and As(V) concentrations were 50 mg/L respectively, MSD dosage 0.2 g, pH 6.0±0.2.)

Fig. 6 Adsorption isotherms for Cr(VI) and As(V) at different temperatures. (MSD dosage 0.5g, pH 6.0±0.2)

Fig. 7 Effect of co-existing anions on Cr(VI) and As(V) removal by MSD. (MSD dosage 0.2g, pH 6.1~7.2, temperature 25±2 °C.)

Fig. 8 Cr(VI) and As(V) breakthrough behavior of the column tests at different bed depths. (Initial Cr(VI) and As(V) concentrations were 10 and 2.5 mg/L respectively, pH 6.0±0.2, temperature 25±2 °C)

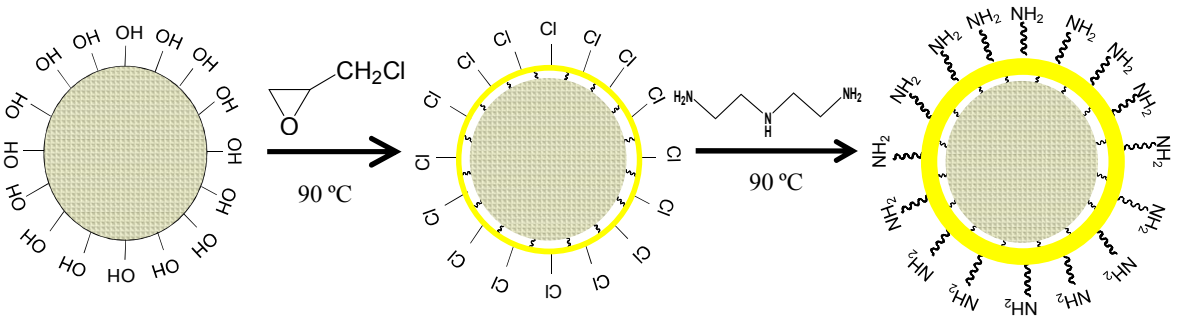

Fig. 1 Schematic diagram of the synthesis process of MSD.

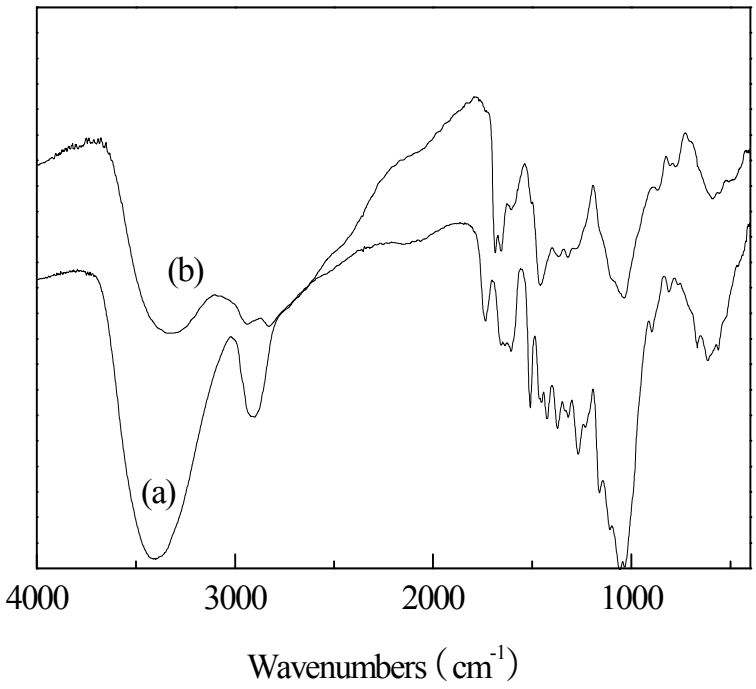

Fig. 2 FT-IR spectra of (a) Raw sawdust and (b) MSD.

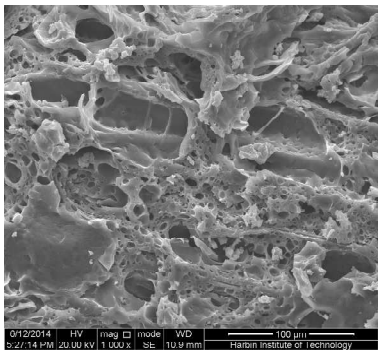

(a) Raw sawdust (×1000)

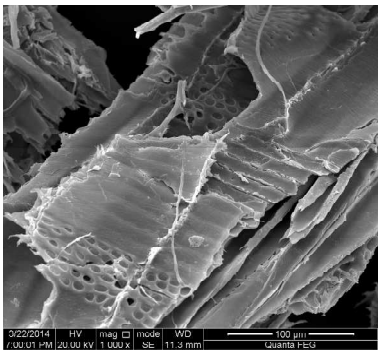

(b) MSD (×1000)

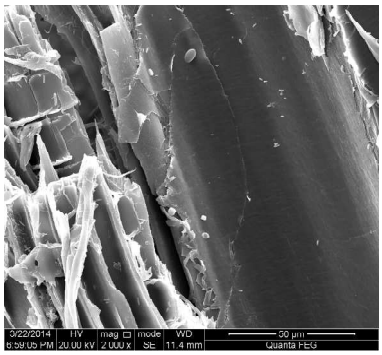

(a) Raw sawdust (×2000)

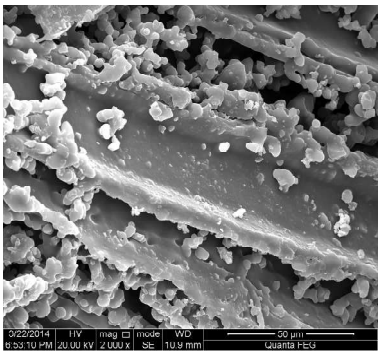

(b) MSD (×2000)

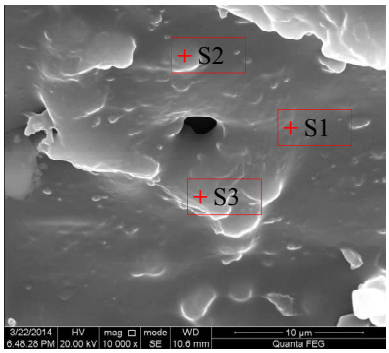

(b) MSD (×10000)

Fig. 3 SEM images of raw sawdust and MSD.

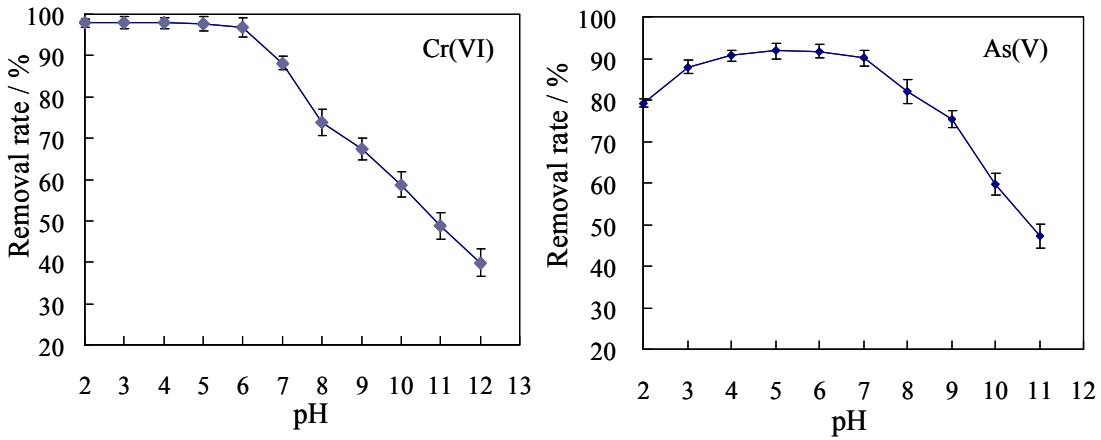

Fig. 4 Effect of pH on Cr(VI) and As(V) removal by MSD. (Intial Cr(VI) and As(V) concentration were 100 mg/L and 50 mg/L respectively, MSD dosage 0.2g, temperature 25±2 °C.)

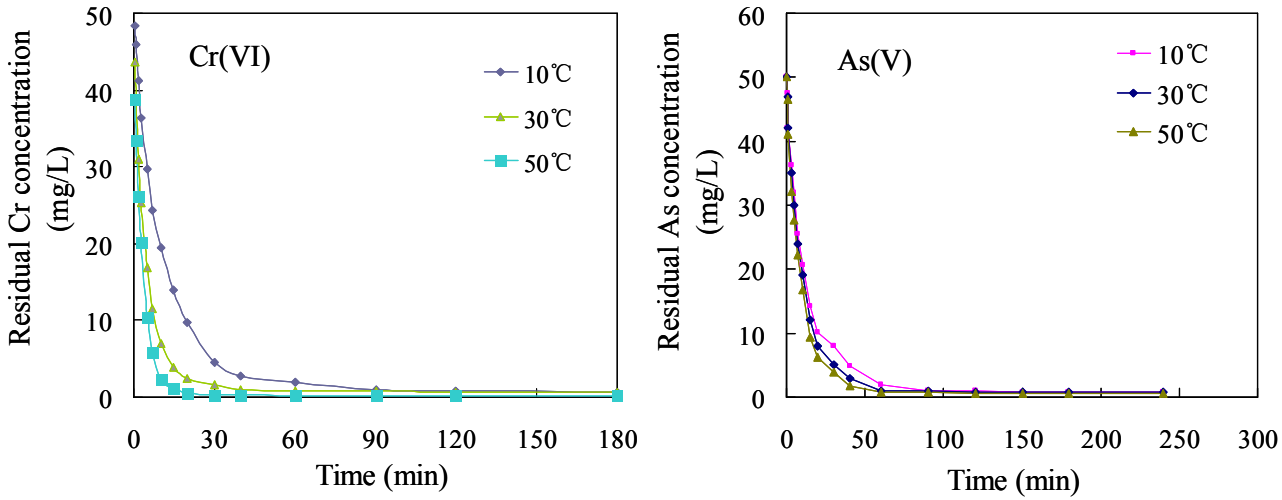

Fig. 5 Adsorption kinetics of Cr(VI) and As(V) by MSD at different temperatures. (Initial Cr(VI) and As(V) concentrations were 50 mg/L respectively, MSD dosage 0.2 g, pH 6.0±0.2.)

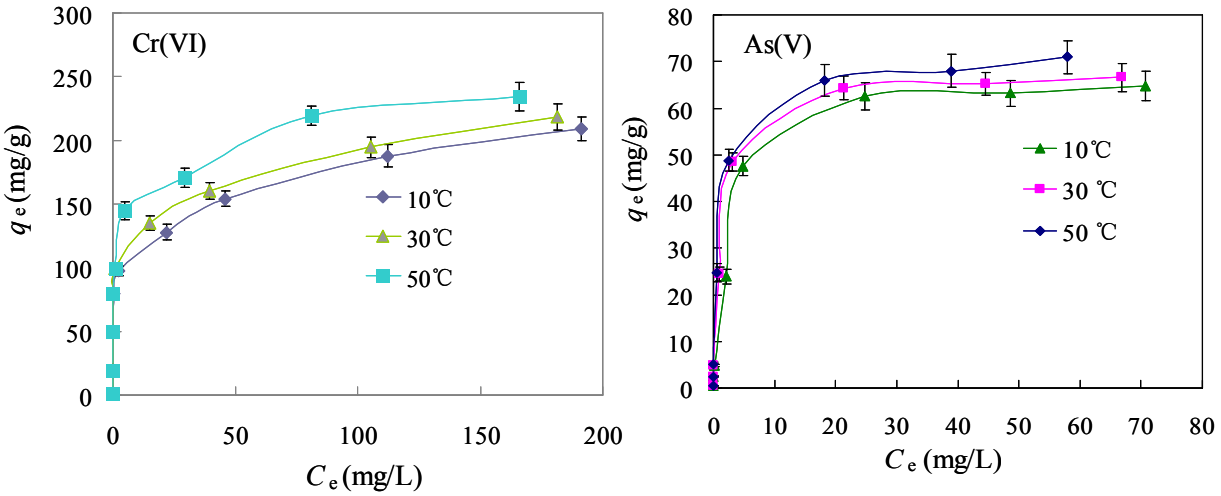

Fig. 6 Adsorption isotherms for Cr(VI) and As(V) at different temperatures. (MSD dosage 0.5g, pH 6.0±0.2)

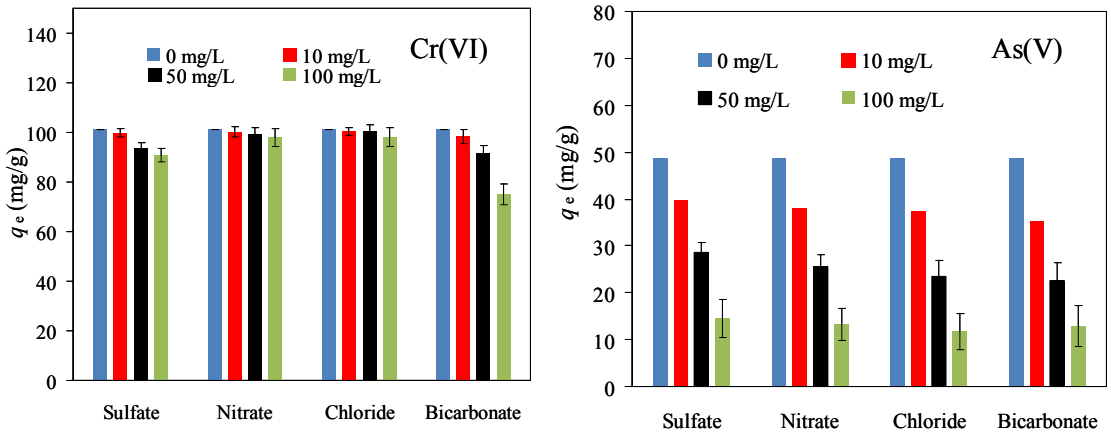

Fig. 7 Effect of co-existing anions on Cr(VI) and As(V) removal by MSD. (MSD dosage 0.2g, pH 6.1~7.2, temperature 25±2 °C.)

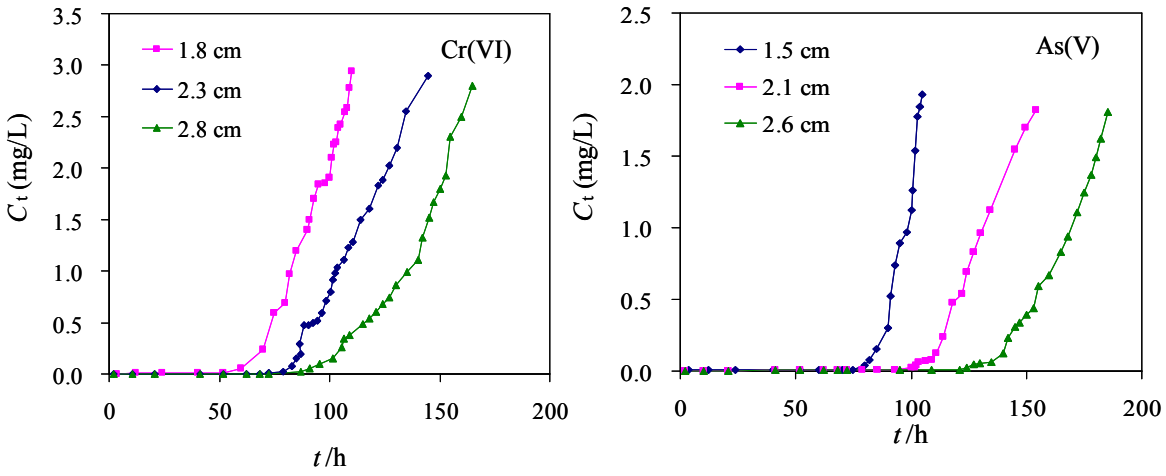

Fig. 8 Cr(VI) and As(V) breakthrough behavior of the column tests at different bed depths. (Initial Cr(VI) and As(V) concentrations were 10 and 2.5 mg/L respectively, pH 6.0±0.2, temperature 25±2 °C)